Field dependence of the *n*-value and its relation with the critical current of Nb_3Sn strands

2007 Supercond. Sci. Technol. 20 851

(http://iopscience.iop.org/0953-2048/20/8/022)

Supercond. Sci. Technol. **20** (2007) 851–858 doi:10.1088/0953-2048/20/8/022

Field dependence of the *n*-value and its relation with the critical current of Nb_3Sn strands

Sangjun Oh[1], Chulhee Lee[1], K W Cho[1], Keeman Kim[1], D Uglietti[2] and R Flükiger[3]

[1] National Fusion Research Center, Daejeon 305-333, Korea
[2] Group of Applied Physics, University of Geneva, Geneva, Switzerland
[3] Department of Solid State Physics and with MANEP (NCCR), University of Geneva, Geneva, Switzerland

E-mail: wangpi@nfrc.re.kr

Received 12 April 2007, in final form 12 June 2007
Published 23 July 2007
Online at stacks.iop.org/SUST/20/851

Abstract
We find a simple expression for the field dependences of the *n*-value for Nb_3Sn strands which gives reasonable fits to empirical data. It is also found that a relationship between the *n*-value and the critical current, which is obtained from an assumed reduction of the flux line lattice shearing pinning force due to thermal activation, can describe the field dependence of the critical current. Using the relation between the *n*-value and the critical current, we propose a scaling law which we have called the Kramer model including thermal activation. It is shown that the proposed scaling law can explain the critical current data at 4.2 K, even at high field near the upper critical field. It is also compared with Ekin's strain scaling law.

1. Introduction

Recent large scale magnet applications and developments in high field NMR magnets have revived interest in the field, temperature and strain dependences of the critical current for Nb_3Sn superconducting strands and appropriate scaling laws for flux pinning [1–3]. The critical current of a superconducting strand is determined by a balance between the Lorentz force and the dynamic pinning force, and is usually defined as a current at which an electric field of 1×10^{-6} V m^{-1} is measured in the electric field–current density (E–J) characteristic curve. The E–J characteristics are known to be described by the empirical power law $E = \alpha J^n$ and the *n*-value is generally regarded as a quality index. Along with the critical current, the *n*-value varies as a function of field, temperature and strain. Recently, Taylor and his co-workers reported on a relationship between the *n*-value and the critical current for a variety of Nb_3Sn strands, but there is no consensus yet on an appropriate framework for the field, temperature and strain dependence of the *n*-value [4, 5].

In this work we present an empirical expression for the field dependence of the *n*-value which is compared with reported results. In section 3, we further obtain a relationship between the *n*-value and the critical current from an assumption that the flux line lattice shearing pinning force is reduced by thermal activation. The possibility of using the relationship between the *n*-value and the critical current as a scaling law for flux pinning is discussed in section 4.

2. Field dependence of the *n*-value

The field dependences of the *n*-value for Nb_3Sn strands at various temperatures and strains reported by Taylor *et al* [6] are shown in figure 1. The vacuumschmelze (VAC) strand is a bronze-route strand (VAC I) and was heat treated at 570 °C for 220 h and at 650 °C for 175 h. The EM-LMI and OST strands are an internal-tin processed and a modified jelly-roll Nb_3Sn wire, respectively. The *n*-value for the VAC I strand shows saturated behaviour at low field and temperature and drops rapidly at high field near the upper critical field, while that for the EM-LMI and OST strands does not saturate at low field and increases gradually as the field is lowered. We found that these different features in the field dependences of the *n*-value for Nb_3Sn strands can be described by a single expression,

$$n(B, T, \varepsilon) = n_0 e^{-\exp(-a(T,\varepsilon)\{1-B/B_n(T,\varepsilon)\})}. \quad (1)$$

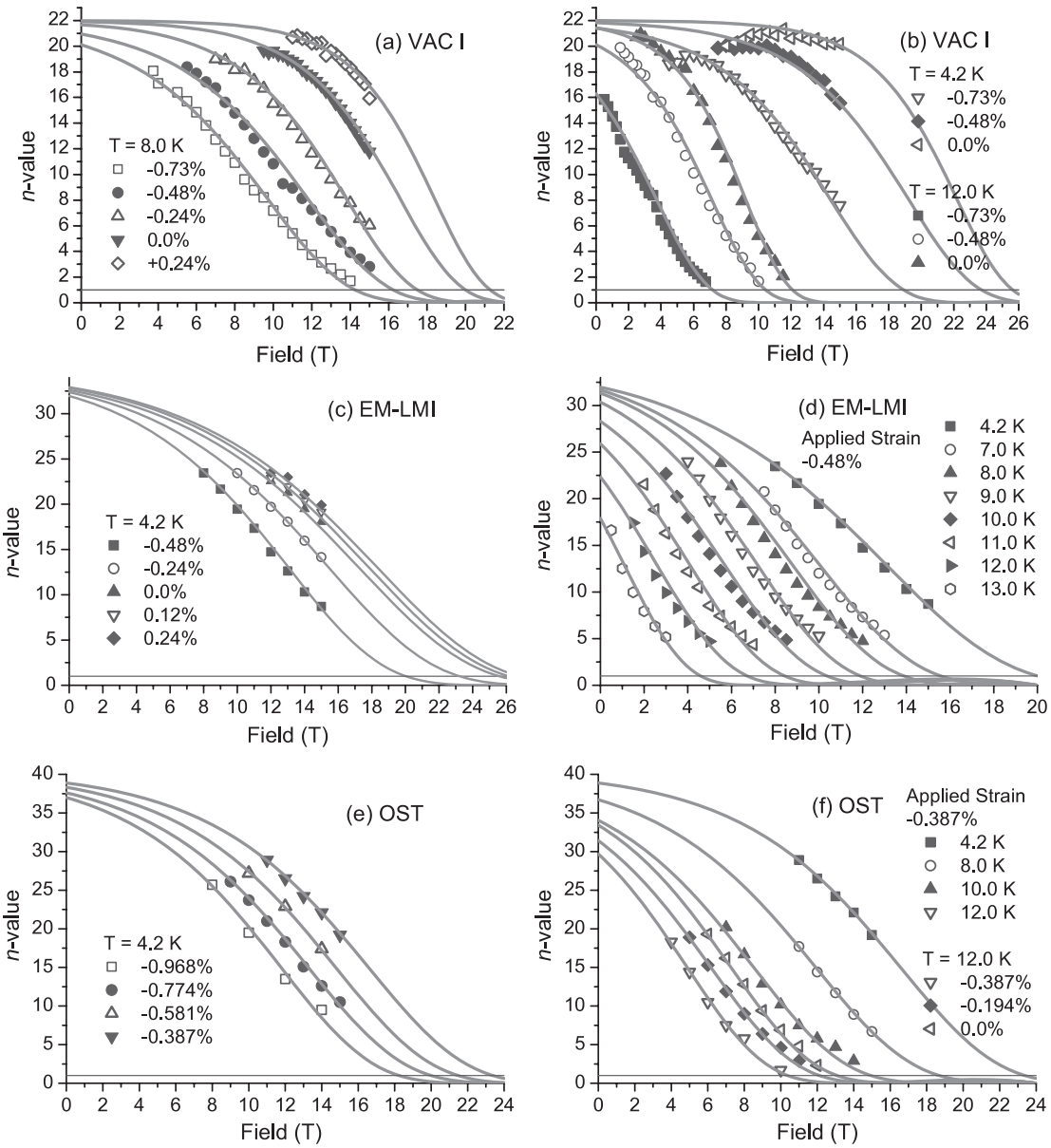

Figure 1. The field dependences of the n-value at various temperatures and strains for the VAC I, EM-LMI and OST strands [6]. Solid lines are the fitting results with (1).

Solid lines in figure 1 are calculated using (1) and are in good agreement with the empirical data. Other data reported by Taylor *et al* can be fitted with (1) as well.

The parameter n_0 used for the fitting is 22.0, 35.0 and 40.5 for VAC I, EM-LMI and OST, respectively. The fit parameters a and B_n at various temperatures and strains are presented in figure 2. With increasing compressive strain, the parameters a and B_n decrease but the variation of a for VAC I is much more pronounced than for the other strands. The temperature dependences of a for EM-LMI and OST are also quite different. As temperature decreases, the parameter a for the OST strand with an applied strain of -0.387% increases almost linearly, while for the EM-LMI strand with a strain of -0.48% it saturates below 8 K. The origin of variations in the n-value is generally attributed either to inhomogeneity of the pinning force (intrinsic effects) or to the variation in the cross-sectional area (extrinsic effects) [5]. The differences in the fitting value of n_0 and the strain and temperature dependences of a might be attributed to either intrinsic effects or extrinsic effects. The parameters n_0, a and B_n may be useful for assessing the contribution of each effect.

The effectiveness of (1) for the description of the n-value for other Nb_3Sn strands needs to be confirmed by further comparative studies. In this work, the n-value for another VAC binary bronze-route strand (VAC II), which was heat treated at 590 °C for 80 h and at 680 °C for 80 h, has been measured at 4.2 K with magnetic field up to 21 T. Details of the measurement procedure using a modified Walters spiral are reported elsewhere [7]. As can be seen in figure 3, the field dependence of the n-value for the VAC II strand can also be

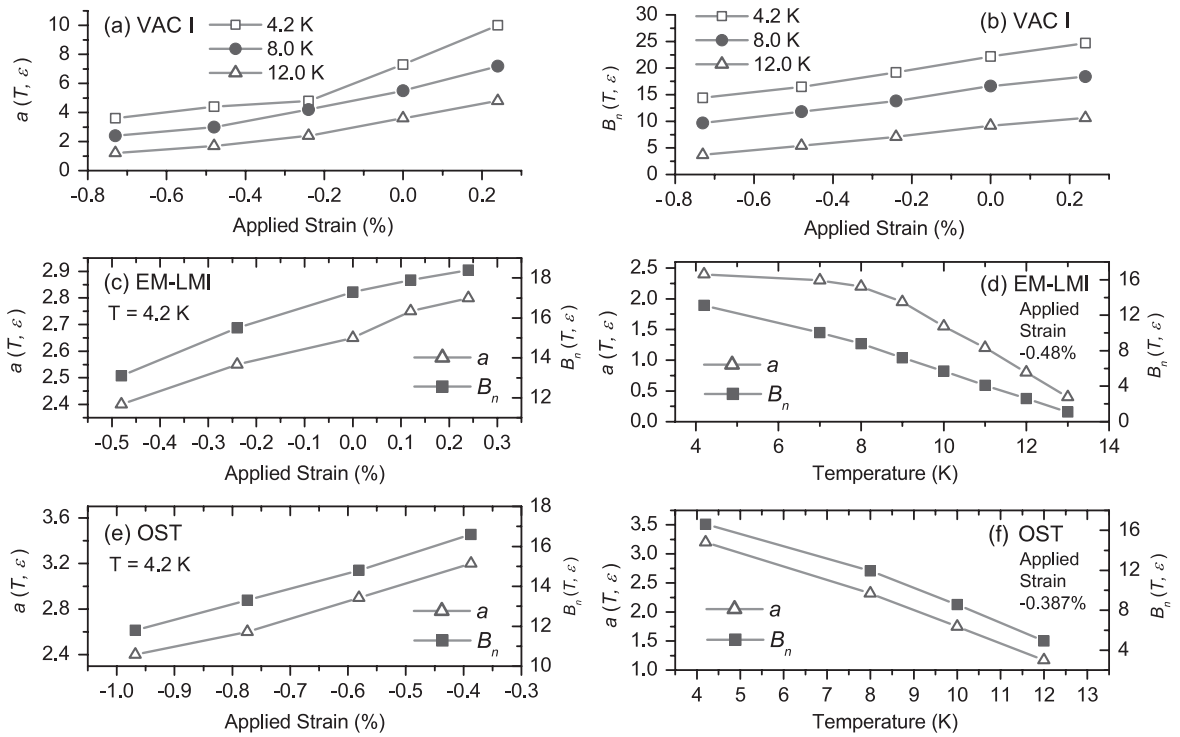

Figure 2. The fitting parameters a and B_n at various temperatures and strains for the VAC I, EM-LMI and OST strands.

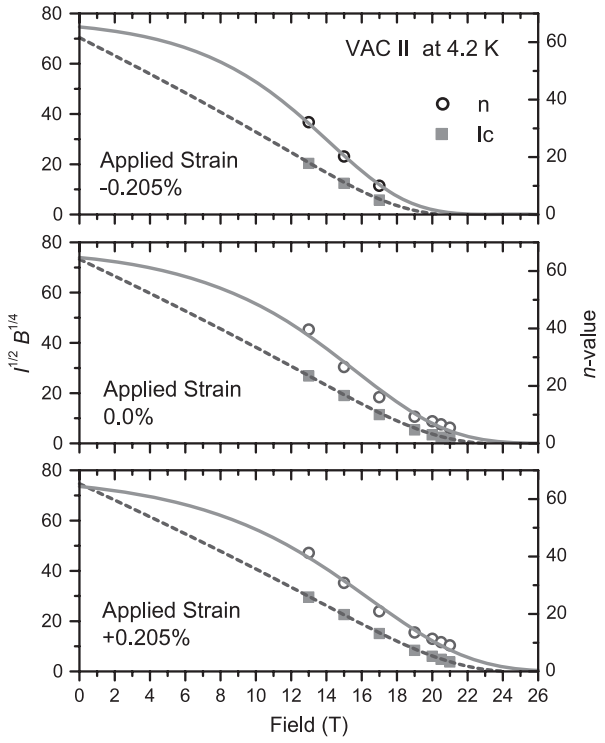

Figure 3. The field dependence of the n-value at 4.2 K for VAC II. Solid lines are the fitting results with (1). To show the relation between the n-value and the critical current, Kramer plots are drawn together. Dotted lines are calculated using (2).

described with (1). The fitting parameter n_0 for VAC II is 68.0 and the values of a and B_n are presented in figure 4.

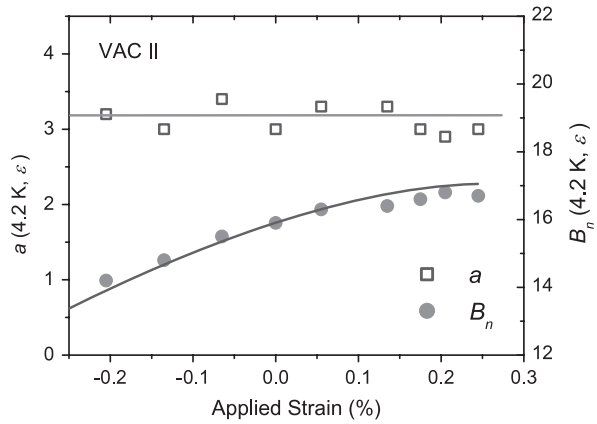

Figure 4. The fitting parameters a, B_n at 4.2 K with various applied strains for VAC II. Solid lines are fitting lines for the strain dependence of a and B_n.

3. Relation between the n-value and the critical current

The power law E–J characteristic, $E = \alpha J^n$, from which the n-value is defined, is reported to occur in high temperature superconductors as well, and is interpreted as flux creep over a logarithmic barrier $U(J) = U_0 \ln(J_c/J)$, especially when the pinning properties are dominated by the effects of planar pins [8]. The flux motion along the direction of the Lorentz force generates an electric field $\boldsymbol{E} = (1/c)\boldsymbol{B} \times \boldsymbol{v}$, where $\boldsymbol{v}$ is the average velocity of the flux lines. The average velocity $\boldsymbol{v}$ is associated with thermally activated jumps of flux lines and can be written as $v = v_0 \exp(-U(J)/k_B T)$. In this respect, the n-

value is related to the activation energy as $n = U_0/k_BT$ [9]. In the Kramer's flux line lattice (FLL) shearing model, the dynamic pinning force is proportional to the elastic energy stored in the FLL, and for a set of strong planar pins the pinning force can be written as $F = I_c \times B = F_m f(b) = F_m b^p(1-b)^q$, with $p = 0.5$, $q = 2$. The reduced field b is defined as a ratio between the applied field and the upper critical field, $b = B/B_{c2}$. Now, we make a simple assumption that the elastic energy stored in the FLL or the dynamic pinning force is reduced by thermal activation; at $T = 0$ K there is no reduction, and at elevated temperature the reduction is given by the ratio between the activation energy and temperature U_0/k_BT or by the n-value. An Arrhenius relation is assumed:

$$I_c \times B = \left(1 - \exp\left[-\frac{n(B,T,\varepsilon)-1}{n(0,0,0)-1}\right]\right) \Big/ (1-e^{-1}) \times F_m(T,\varepsilon) f(b) \quad (2)$$

where $f(b) = b^{0.5}(1-b)^2$. A FLL shearing model including thermal activation has already been considered for high temperature superconductors with the Anderson–Kim model activation energy [10]. When $n = 1$, the power law E–J characteristic, $E = \alpha J^n$, becomes simple resistive and $n = 1$ can be regarded as a point at which the critical current vanishes. In (2), the ratio of $(n-1)$ instead of n is used.

In figure 3, the field dependence of the critical current is also presented in the form of Kramer plots. Dotted lines are calculated with (2) using (1) for the field dependence of the n-value. The values of the fitting parameters B_{c2} and F_m are shown in figure 5. The relation (2) is an effective expression for describing the field dependence of the critical current, as can be more clearly seen in figure 6. Kramer plots for VAC I, EM-LMI and OST are shown in figure 6 and solid lines are calculation results with (2). For the calculation with (2), the following functional form of $f(b)$ is used:

$$f(b) = b^{1/2}[g(1-b)^{-2}\{1-(1+(1-b)^4/g)e^{-(1-b)^4/g}\} + (1-b)^2 e^{-(1-b)^4/g}] \quad (3)$$

where g is the ratio of the average pin-breaking dynamic pinning force to the FLL shearing force. In our previous work, we reported that the low-field concave part in the Kramer plots can be consistently understood if we also consider the pin-breaking dynamic pinning force together with the FLL shearing force [11]. Previous fitting results without consideration of thermal activation are shown in figure 6(a) as dotted lines, where a parameter g of 1.5 was used. All solid lines in figure 6 were calculated with the same value of g. Compared with the previous fitting results, solid lines shown in figure 6(a) are in better agreement with the data, especially near the upper critical field. The fitting parameters F_m and B_{c2} are quite different for the solid and dotted lines in figure 6(a). For example, at 8 K with an applied strain of -0.73%, F_m and B_{c2} for the solid line are 2200 T A and 14.0 T, respectively, while for the dotted line they are 2020 T A and 11.9 T. A B_{c2} value of 14.0 T seems to be more reasonable extrapolated upper critical field at 8 K with -0.73% strain.

The dotted lines in figure 6(b) are calculated with the same values of F_m and B_{c2} used for the fitting with (2) (solid lines in figure 6(b)). However, we set $n(B,T,\varepsilon)$ to $n(0,0,0)$; in other words the 'thermal activation term' in (2) is removed. Our interpretation is that due to thermal activation, the critical current represented by the dotted lines in figure 6(b) is reduced to the value represented by the solid lines. In this interpretation, at 4.2 K, the reduction term due to thermal activation is only effective near the upper critical field, while at 12 K it is effective at all fields. The 'positive curvature' in Kramer plots near the upper critical field was usually attributed to microstructural or compositional inhomogeneities. Recently, Cooley *et al* reported that the 'positive curvature' can be understood by compositional gradients from model calculations for a powder-in-tube processed strand [12]. The pinning force reduction due to thermal activation might be another possible explanation for the observed 'positive curvature' in Kramer plots.

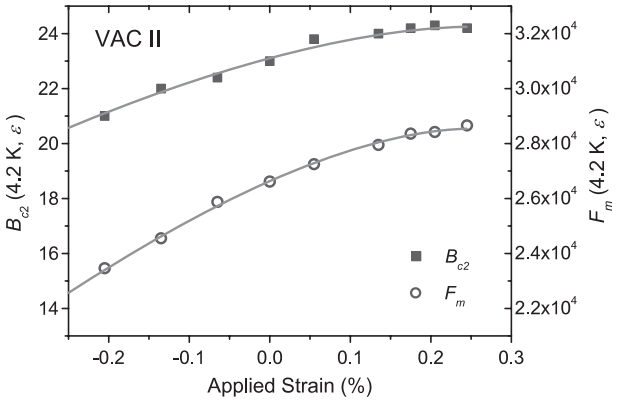

Figure 5. The fitting parameters B_{c2} and F_m at 4.2 K with various applied strains for VAC II. Solid lines are calculated with (6).

The strain dependence of parameters B_{c2} and F_m used for the calculation of solid lines in figure 6(c) to fit the EM-LMI strand data at 4.2 K with (2) and the temperature dependence of B_{c2} and F_m used to fit the EM-LMI data at -0.48% applied strain (solid lines in figure 6(d)) are shown in figures 7 and 8. The parameters B^*_{c2} and F^*_m obtained from conventional linear extrapolation (dotted lines in figures 6(c) and (d)) are also presented in figures 7 and 8. The strain dependence of B^*_{c2} and F^*_m is in agreement with Ekin's strain scaling law [13]. Ekin's strain scaling law at 4.2 K can be written as

$$I_c \times B = F^*_m b^p (1-b)^q, \qquad F^*_m \propto (B^*_{c2})^m, \qquad B^*_{c2}(\varepsilon) = B^*_{c2}(0)(1-c|\varepsilon|^{1.7}) \quad (4)$$

where ε is an intrinsic strain, defined as $\varepsilon = \varepsilon_{applied} - \varepsilon_{max}$. ε_{max} is a strain where the strain dependence of the critical current shows its maximum and for EM-LMI it is about 0.32%. In Ekin's strain scaling law, p, q are arbitrary fitting parameters and the conventional linear extrapolation corresponds to $p = 0.5$, $q = 2$. The pinning force maximum F^*_m is almost proportional to the extrapolated upper critical field B^*_{c2} ($m = 1$) and the best fit is obtained with $c = 1150$, $B^*_{c2}(0) = 25.5$ T and $F^*_m(0) = 9700$ T A (dotted lines in figure 7).

On the other hand, the pinning force maximum F_m obtained with (2) is not proportional to B_{c2} but is proportional to $(B_{c2})^{1.33}$ ($m = 1.33$). We found that the overall strain and temperature dependences of B_{c2} and F_m are in agreement with the results of recent theoretical calculations based on strong coupling theory of superconductivity [3]. It was

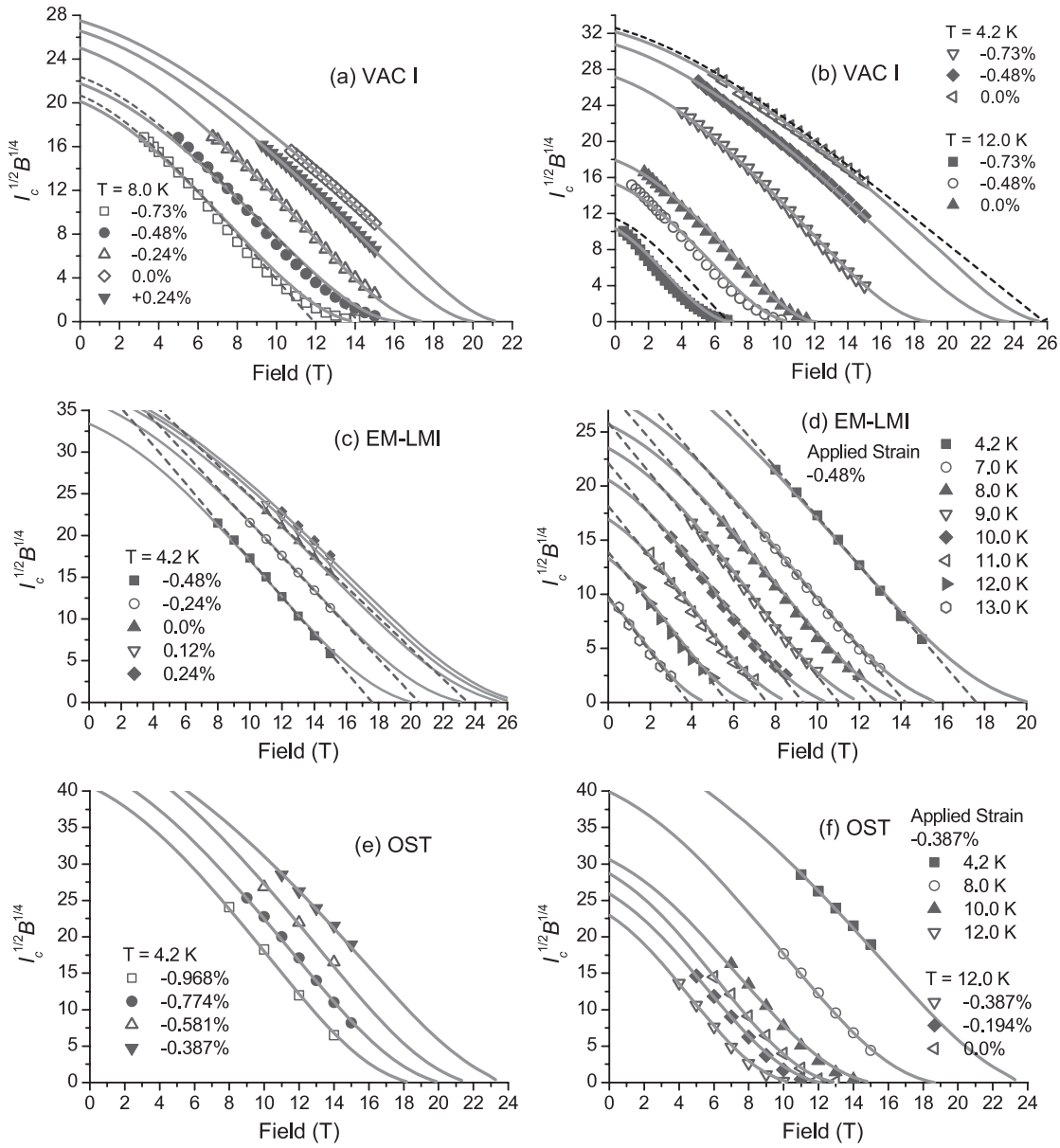

Figure 6. Kramer plots for VAC I, EM-LMI and OST [6]. All solid lines are calculated using equations (2) and (3). Dotted lines in (a) are fitting results calculated with (3) [11]. Dotted lines in (b) are calculated with (2) using the same parameters, F_m and B_{c2} for the solid lines but without the thermal activation term. Dotted lines in (c) and (d) are fitting results with $f(b) = b^{0.5}(1-b)^2$.

shown that if the strain dependence of the critical temperature can be described by $T_c(\varepsilon) = T_c(0)(1-\alpha|\varepsilon|^{1.7})$, then the thermodynamic critical field can be written as $B_c(T,\varepsilon) = B_c(0,0)(1-\beta|\varepsilon|^{1.7})(1-t^{2.17})$, with $t = T/T_c$. It was further reported that the upper critical field B_{c2} and the pinning force maximum F_m can be expressed as [3]

$$\begin{aligned} B_{c2}(T,\varepsilon) &= B_{c2}(0,0)(1-\beta|\varepsilon|^{1.7}) \\ &\quad\times (1-\gamma|\varepsilon|^{1.7})(1-t^{2.17})k(t,\varepsilon) \\ F_m(T,\varepsilon) &= F_m(0,0)(1-\beta|\varepsilon|^{1.7})^{5/2} \\ &\quad\times (1-\gamma|\varepsilon|^{1.7})^{1/2}(1-t^{2.17})^{5/2}k(t,\varepsilon)^{1/2} \end{aligned} \tag{5}$$

where

$$k(t,\varepsilon) = \left(1+u\frac{1-\gamma|\varepsilon|^{1.7}}{1-\alpha|\varepsilon|^{1.7}}(1-t^v)\right)\Big/\left(1+u\frac{1-\gamma|\varepsilon|^{1.7}}{1-\alpha|\varepsilon|^{1.7}}\right).$$

The coefficients α, β and γ are related to the strain dependence of the critical temperature T_c, the thermodynamic critical field B_c and the Ginzburg–Landau parameter, respectively, and the parameters u and v describe the temperature dependence of the Ginzburg–Landau parameter or the upper critical field B_{c2}.

At 4.2 K, (5) can be approximated as

$$\begin{aligned} B_{c2}(4.2\text{ K},\varepsilon) &\approx B_{c2}(4.2\text{ K},0)(1-\beta|\varepsilon|^{1.7})(1-\gamma|\varepsilon|^{1.7}) \\ F_m(4.2\text{ K},\varepsilon) &\approx F_m(4.2\text{ K},0)(1-\beta|\varepsilon|^{1.7})^{5/2} \\ &\quad\times (1-\gamma|\varepsilon|^{1.7})^{1/2}. \end{aligned} \tag{6}$$

Solid lines in figure 7 are calculated with (6) and the best fit is obtained with parameters of $B_{c2}(4.2\text{ K},0) = 28.4$ T,

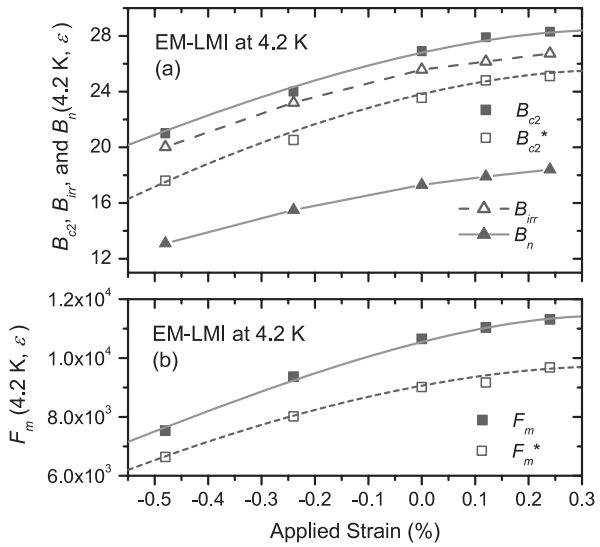

Figure 7. The strain dependence of the fitting parameters B_{c2}, B^*_{c2}, B_n, F_m and F^*_m. B_{c2} and F_m are the parameters used for the calculation of solid lines in figure 6(c). B^*_{c2} and F^*_m are obtained from conventional linear extrapolation (dotted lines in figure 6(c)). The parameter B_n shown in figure 2(c) is also shown, for comparison. The irreversibility field B_{irr} was calculated from a and B_n. Solid lines are calculated with (6).

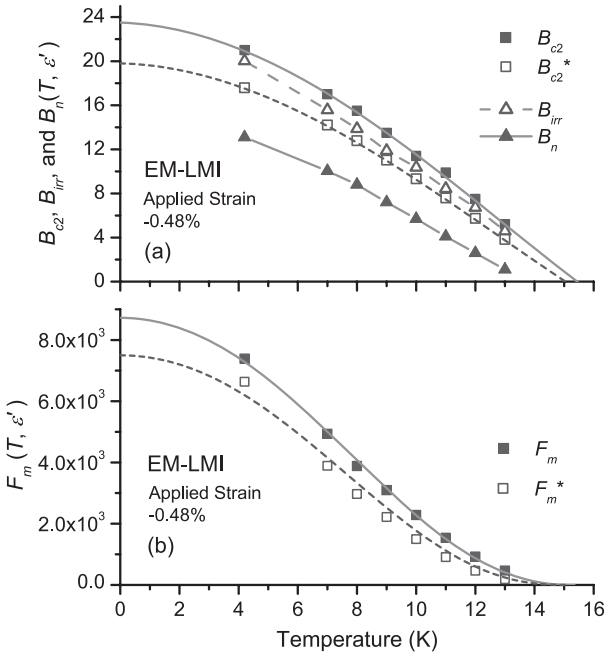

Figure 8. The temperature dependence of the fitting parameters B_{c2}, B^*_{c2}, B_n, F_m and F^*_m. B_{c2} and F_m are the parameters used for the calculation of solid lines in figure 6(d). B^*_{c2} and F^*_m are obtained from conventional linear extrapolation (dotted lines in figure 6(d)). The parameter B_n shown in figure 2(d) is also given for comparison. The irreversibility field B_{irr} was calculated from a and B_n. Solid lines are calculated with (7).

$F_m(4.2\ \mathrm{K}, 0) = 11\,430$ T A, $\beta = 440$ and $\gamma = 560$. Incidentally, the coefficients $\beta = 440$ and $\gamma = 560$ correspond to the calculation results for the phonon anharmonicity model at low impurity concentration (case I of [3], at $\pi t_+ = 10$ K). The estimated values of α, β, γ, u and v from the theoretical calculations are 321, 441, 559, 0.66 and 1.5, respectively. At fixed strain ($\varepsilon = \varepsilon'$), equations (5) reduce to

$$B_{c2}(T, \varepsilon') = B_{c2}(0, \varepsilon')(1 - t^{2.17})\{(1 + u't^v)/(1 + u')\}$$
$$F_m(T, \varepsilon') = F_m(0, \varepsilon')(1 - t^{2.17})^{5/2}\{(1 + u't^v)/(1 + u')\}^{1/2} \quad (7)$$

with $u' = u(1 - \gamma|\varepsilon'|^{1.7})/(1 - \alpha|\varepsilon'|^{1.7})$. Solid lines in figure 8 calculated with (7) using α, β, γ, u and v from the theoretical calculations are in good agreement with the data. Only $T_c(\varepsilon')$, $B_{c2}(0, \varepsilon')$ and $F_m(0, \varepsilon')$ are used as fitting parameters and the best fit is obtained with $T_c(\varepsilon') = 15.45$ K, $B_{c2}(0, \varepsilon') = 23.5$ T and $F_m(0, \varepsilon') = 8720$ T A. As shown in figure 8(a) as a dotted line, the temperature dependence of B^*_{c2} obtained from the conventional linear extrapolation can also be described with (7) using the same α, β, γ, u and v but with a slightly lower values of $T_c(\varepsilon')$ and $B_{c2}(0, \varepsilon')$, 19.8 T and 15.05 K, respectively. However, the dotted line calculated with (7) using the same values of α, β, γ, u and v shows more deviation from the temperature dependence of F^*_m compared with the solid line in figure 8(b).

In figures 7(a) and 8(a), the parameter B_n for EM-LMI shown in figures 3(c) and (d) are drawn together, for comparison. As noted, the physical meaning of the parameter B_n is unclear at the moment, but from a and B_n, the field at which $n = 1$, or the irreversibility field B_{irr}, can be calculated as shown in figures 7(a) and 8(a). From the magnetization measurement of a 2 at.% Ti added ternary Nb_3Sn strand, Suenaga *et al* reported on the irreversibility field for a wide range of temperatures [14]. The irreversibility fields obtained in this work are larger than the upper critical fields B^*_{c2} obtained from the conventional linear extrapolation and a bit lower than the upper critical fields B_{c2} obtained from the fitting with (2).

Equation (2) is not a rigorous relation. However, it can be regarded as an effective functional form for the relation between the n-value and the critical current. A relationship between the n-value and the critical current is also reported by Taylor *et al* in the form of a modified power law, $n = 1 + r(I_c)^s$, where r and s are functions of temperature and strain [5]. In the next section, the effectiveness of the scaling law incorporating (2), which we tentatively call the Kramer model including thermal activation, is further discussed.

4. A scaling law based on the Kramer model including thermal activation

If we summarize the previous sections, the pinning force is reduced due to thermal activation which can be parameterized by the n-value as (2), and the field dependence of the n-value can be expressed by (1). If we are to use (2) as a scaling law and to calculate the critical current we need to know about the strain and temperature dependences of the n-value as well. For VAC II, we can easily find the strain dependences of a and B_n as can be seen in figure 4. The values of a are almost independent of strain and can be approximated as a constant, $a\ (4.2\ \mathrm{K}, \varepsilon) = 3.2$, while the strain dependence B_n can be approximated by $B_n(4.2\ \mathrm{K}, \varepsilon) = 16.75\ \mathrm{T} \times (1 - 1450|\varepsilon|^{1.7})$. Here ε is an intrinsic strain as defined in the previous section, $\varepsilon = \varepsilon_{applied} - \varepsilon_{max}$, and ε_{max} for the VAC II strand is about

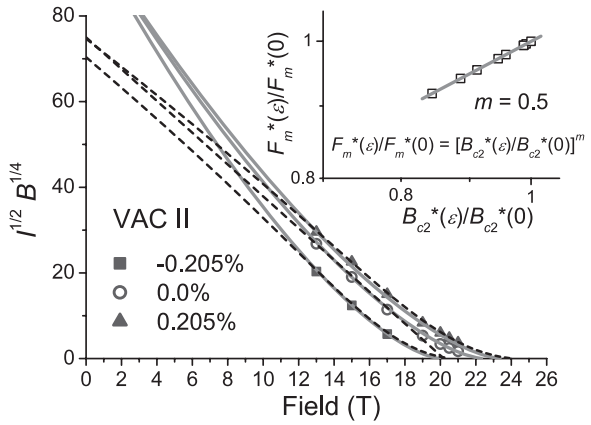

Figure 9. Kramer plots for VAC II. Solid lines are calculated with Ekin's strain scaling law with $p = 0.5$, $q = 3$. The upper and lower dotted lines are calculated with (2). The dotted line in the middle is a fitting result with $f(b) = b^{0.5}(1-b)^2$. Inset: the relation between F_m^* and B_{c2}^* when $p = 0.5$, $q = 3$.

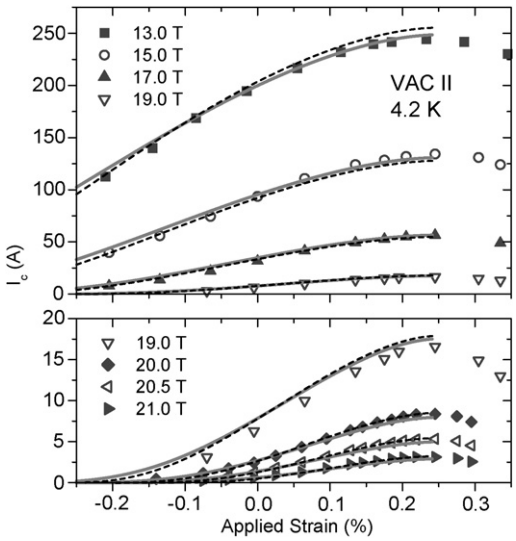

Figure 10. The strain dependence of the critical current for strand VAC II. Solid lines are calculated with the Kramer model including thermal activation. Dotted lines are calculated with Ekin's strain scaling law (4) with $p = 0.5$, $q = 3$.

0.245%. Even though the VAC II strand is measured only at 4.2 K, as shown in figure 6(b), if the pinning force is reduced by the thermal activation effect, we can see the effect near the upper critical field. Figure 9 is an enlarged Kramer plot for VAC II and the fitting results with (2) for applied strain of −0.205% and 0.205% are shown together as dotted lines (the upper and lower dotted lines). It is clear that the data near the upper critical field cannot be described by $f(b) = b^p(1-b)^q$, with $p = 0.5$, $q = 2$ (the linear dotted line in the middle).

In our previous work, it was shown that the Kramer model can explain the strain dependence of the critical current at 4.2 K [11], if the calculation results based on strong coupling theory of superconductivity are used [3]. The strain dependences of B_{c2} and F_m for VAC II can be calculated with (6) and the best fit is obtained with the values of the parameters B_{c2} (4.2 K, 0) = 24.3 T, F_m (4.2 K, 0) = 28 540 T A, $\beta = 610$ and $\gamma = 700$ (solid lines in figure 5). The critical currents calculated with (2) using the parameters listed above are shown in figure 8 as solid lines which represent the empirical data pretty well, even at a high field of more than 20 T. At least, from an engineering point of view, we can argue that the Kramer model including thermal activation is effective, especially near the upper critical field.

For comparison, the critical current of VAC II is also analysed with (4), Ekin's strain scaling law at 4.2 K [13]. As noted, in Ekin's strain scaling law p, q are the fitting parameters and the best fits are obtained with $p = 0.5$, $q = 3$ as shown in figure 9. Dotted lines in figure 10 are the calculation results with (4) using the parameters $B_{c2}^*(0) = 23.7$ T, $F_m^*(0) = 48\,700$ T A, $c = 1550$ and $m = 0.5$. It is also in good agreement with the measured critical current and it should be noted that the fitting parameter $q = 3$, and especially $m = 0.5$, might be a result of sample inhomogeneity [15]. Further comparative studies on various Nb_3Sn strands will be needed for an understanding of the positive curvature in the Kramer plot near the upper critical field and for a proper scaling law at high applied field.

5. Conclusions

In summary, we have shown that the field dependences of the n-value for a variety of Nb_3Sn strands can be written in a simple functional form as $n(B, T, \varepsilon) = n_0 e^{-\exp[-a(B/Bn)]}$. It was shown that the parameters n_0, a and B_n are strongly sample dependent which might be attributed either to intrinsic or to extrinsic effects. We argue that the n-value is related to the activation energy, $n = U_0/k_B T$, and make an assumption that the FLL shearing pinning force is reduced due to thermal activation in an Arrhenius relation. The field dependence of the critical current, represented in the form of Kramer plots, can be described by the relationship we obtained from an assumption of thermal activation. The strain and temperature dependence of the fitting parameters B_{c2} and F_m are in agreement with recent theoretical calculation results based on the strong coupling theory of superconductivity. The relationship is further used as a scaling law, and it is shown that the strain dependence of the critical current can be described by the proposed scaling law even at high fields near the upper critical field. However, the positive curvature in the Kramer plot and a scaling of the flux pinning near the upper critical field can also be attributed to the effect of sample inhomogeneity, and further comparative studies are needed.

References

[1] ten Haken B, Godeke A and ten Kate H 1999 *J. Appl. Phys.* **85** 3247
[2] Keys S and Hampshire D 2003 *Supercond. Sci. Technol.* **16** 1097
[3] Oh S and Kim K 2006 *J. Appl. Phys.* **99** 033909
[4] Taylor D, Keys S and Hampshire D 2002 *Physica* C **372–376** 1291
[5] Taylor D and Hampshire D 2005 *Supercond. Sci. Technol.* **18** S297
[6] Taylor D and Hampshire D 2005 *Supercond. Sci. Technol.* **18** S241

[7] Uglietti D, Seeber B, Abächerli V, Thöner M and Flükiger R 2003 *IEEE Trans. Appl. Supercond.* **13** 3544
[8] Yeshurun Y, Malozemoff A and Shaulov A 1996 *Rev. Mod. Phys.* **68** 911
[9] Caplin A, Bugoslavsky Y, Cohen L and Perkins G 2004 *Physica* C **401** 1
[10] Wördenweber R 1998 *Rep. Prog. Phys.* **62** 187
[11] Oh S and Kim K 2006 *IEEE Trans. Appl. Supercond.* **16** 1216
[12] Cooley L, Fischer C, Lee P and Larbalestier D 2004 *J. Appl. Phys.* **96** 2122
[13] Ekin J 1980 *Cryogenics* **20** 611
[14] Suenaga M, Ghosh A, Xu Y and Welch D 1991 *Phys. Rev. Lett.* **66** 1777
[15] Ekin J 1985 *Proc. Int. Symp. on Flux Pinning and Electromagnetic Properties in Superconductors* (Fukuoka: Matsukuma Press) p 267